Investigation of the Wear Resistance of High Chromium White Irons

G.D. Nelson, G.L.F. Powell and V.M. Linton
School of Mechanical Engineering, The University of Adelaide, South Australia, Australia
grant.nelson@mecheng.adelaide.edu.au, phone: (+61) 08 8303 3152

Key Words
Erosion-corrosion, slurry pot, high chromium white iron, sodium aluminate solution

Abstract

High chromium white irons are commonly used throughout the mineral processing industry to handle erosive and erosive-corrosive slurries. These alloys are used in critical wear areas in the form of castings, or deposited as weld overlays onto steel substrates. The wear resistance of these alloys is due to their microstructure, which comprises hard rod like carbides dispersed in a matrix of austenite or martensite. The microstructure and carbide morphologies of these alloys can vary significantly depending on the chemical composition and the production process.

This investigation uses a simple slurry pot test apparatus with slurries containing a mixed proportion of quartz particles to produce a mixed mode of impact and low angle erosion. A variety of different commercially produced castings and weld overlays ranging from low carbide volume fraction hypoeutectic alloys to hypereutectic alloys having a high carbide volume fraction were tested. The wear mechanism and hence the wear resistance of the alloys tested has been related to the matrix and the carbide morphologies.

Introduction

In many industrial applications coarse ore is ground in rod or ball mills before being mixed with a liquid to form slurries for economical transfer between processing stages. The slurries generally contain a high proportion of abrasive particles of varying sizes, due to the nature of the crushing process, creating an erosive environment. In order to minimize wear in critical areas, processing components used for the transfer of slurries are either cast or weld overlayed with wear resistant materials. High chromium white iron, in the form of castings and weld overlays, is one of the alloys used to improved wear resistance and equipment longevity.

High chromium white irons are ferrous based with the main alloying additions being 11-35 wt% chromium and 1.8-7.5 wt% carbon [1, 2]. The wear resistance of these alloys stems from the distribution of hard carbides, which form in-situ on cooling from the melt of a casting or molten weld deposit, in a softer ductile matrix. The chemical composition of the alloys can be varied to produce different proportions of carbides, usually expressed as carbide volume fraction (CVF) [3]. The relationship between erosive wear and CVF has been investigated for small size ranges of silica sand particles using a gas blast erosion test rig [4]. However, in many industrial applications the size of the erosive particles entrained within the slurry ranges in size from a high proportion of small particles (<53µm) to a low proportion of large particles (>1.0mm). In specific wear environments, such as in the wet grinding of granite using ball mills, the size and distribution of the abrasive particles have been found to have a significant effect on wear rates, with the highest wear rates occurring when fine particles were present in the highest proportion [5]. However, the effect of having a variable size distribution of abrasive particles in an erosive slurry environment has not been rigorously investigated.

This paper investigates the erosive wear of three high chromium white iron alloys using a slurry pot erosion testing device. The three white irons have distinctly different microstructures or have undergone a heat treatment to alter the properties of the alloy. A fourth alloy, Stellite 6, is included in this investigation to compare the wear resistance and wear mechanism of Stellite against the high chromium white irons, which, depending on product form, have a higher CVF or higher matrix hardness.

Test Materials

The alloys investigated were hypereutectic and hypoeutectic high chromium white iron castings, a hypereutectic high chromium white iron weld overlay deposited on a steel substrate using flux cored arc welding and a hypoeutectic cobalt based Stellite 6 deposited on a steel substrate using plasma transferred arc (PTA) welding. The cast samples and the hypereutectic weld overlay samples were sectioned from worn plant components, and the Stellite 6 sample was sectioned from a bead on plate PTA deposit. The hypereutectic casting, Fig. 1, has a microstructure consisting of large primary M_7C_3 carbides (the M in this case representing a combination of chromium and iron) in a matrix of austenite and a small amount of martensite. The dark regions contained within the austenitic matrix of Fig. 1 are a dense agglomeration of $M_{23}C_6$ carbides. The hypoeutectic casting, Fig. 2, had been heat treated. The as cast hypoeutectic alloy had a microstructure of primary austenite dendrites and an inter-dendritic eutectic of austenite and eutectic M_7C_3 carbides [3]. On heat treatment the austenite is destabilised resulting in the precipitation of $M_{23}C_6$ carbides in a martensitic matrix. The $M_{23}C_6$ carbides are not easily resolved in the figure. The hypereutectic weld overlay, Fig. 3, was deposited onto a steel substrate using the flux-cored arc welding process. The microstructure consists of primary M_7C_3 carbides and a eutectic of austenite and fine eutectic M_7C_3 carbides surrounding the primary carbides. It should be noted that the eutectic M_7C_3 carbides of the weld overlay are much finer than those of the hypoeutectic casting due to the faster cooling rate of the weld overlay.

A commonly encountered problem with hypereutectic high chromium white iron weld overlays is check cracking, Fig. 4. The check cracking is caused by the relieving of residual stresses produced during the solidification and cooling of the molten weld pool. The check cracks generally extend from the surface of the overlay to the substrate-hardfacing interface.

The Stellite 6 deposit, Fig. 5, has a hypoeutectic microstructure of primary dendrites of solid solution cobalt and an inter-dendritic eutectic of solid solution cobalt and eutectic M_7C_3 carbides (the M in this case representing a combination of chromium and cobalt). Unlike the hypereutectic high chromium weld overlays, the PTA deposited Stellite overlays did not contain check cracks.

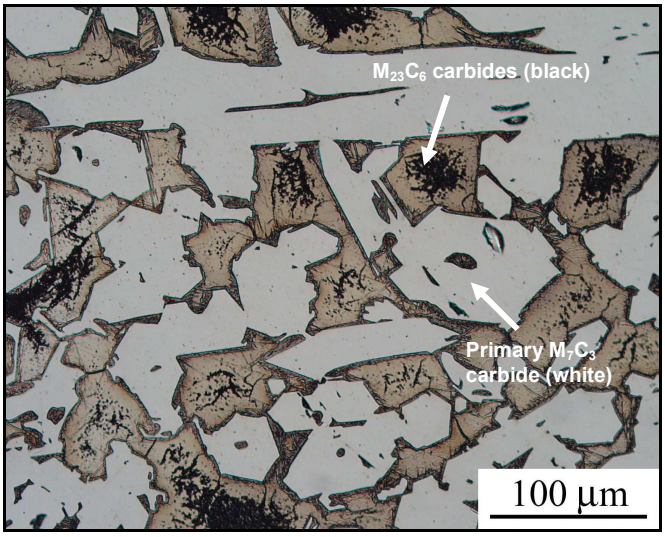

Figure 1: Optical light micrograph of the hypereutectic high chromium white iron casting, 200x, etched in acid ferric chloride.

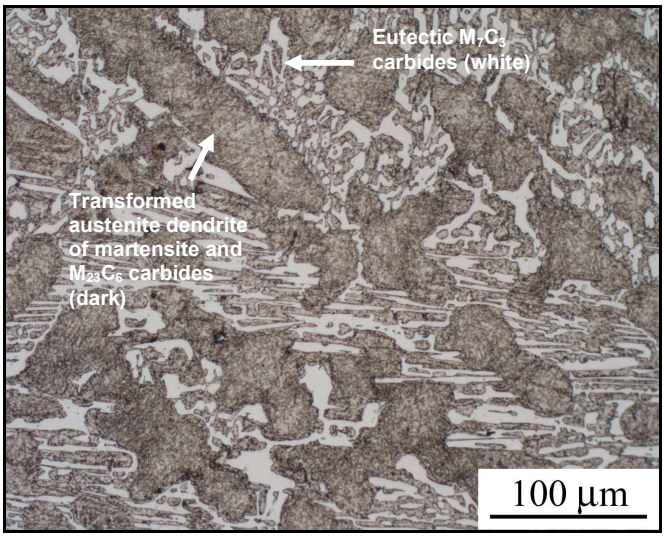

Figure 2: Optical light micrograph of the hypoeutectic high chromium white iron casting that has been heat treated, 200x, etched in acid ferric chloride

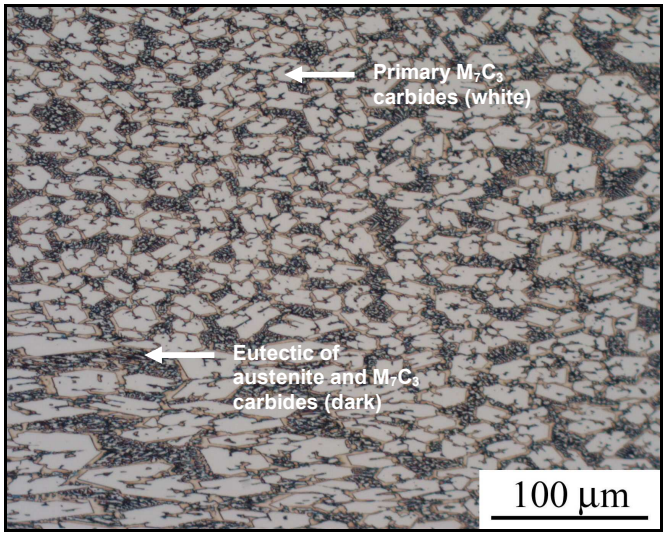

Figure 3: Optical light micrograph of the hypereutectic high chromium white iron weld overlay, 200x, etched in acid ferric chloride.

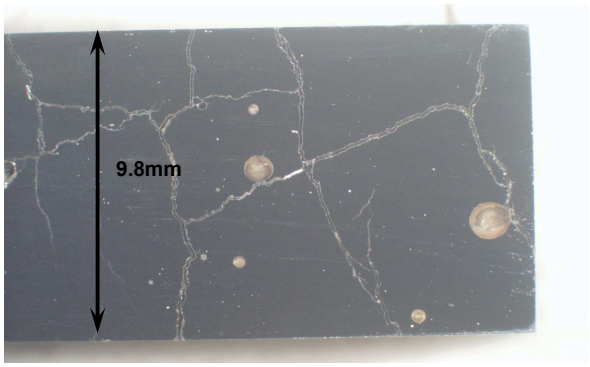

Figure 4: The extent of check cracking of a hypereutectic weld overlay sample.

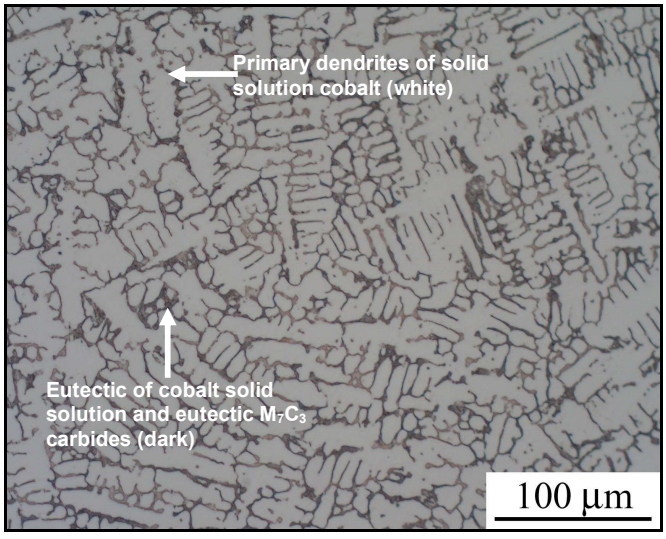

Figure 5: Optical light micrograph of Stellite 6 weld overlay, 200x, 5% HCl electrolytic etch.

Slurry Pot Test Device

The slurry pot testing device used in this work, Fig. 6, was similar to that used by Lathabai and Pender [6]. Six test samples in the form of square bars (9.8±0.1 × 9.8±0.1 × 40.0±0.1 mm) were mounted radially in a circular spindle and securely clamped in the device using nylon screws. The spindle and associated components were constructed from an acetal based engineering polymer that can withstand temperatures up to approximately 100°C. The spindle was coupled to a 0.75 kW variable speed motor and immersed in a 2L polypropylene beaker containing the test slurry. To prevent vortex formation and turbulent flow the beaker had four vertical polypropylene baffles located at 90° to each other to suspend the abrasive particles. The rotational speed of the motor was set using a digital frequency controller to ensure the rotational speed was the same for all tests. The rotational speed was set at 1000 rpm, which corresponds to a wear velocity at the tip of the sample of approximately 5.6 $m.s^{-1}$.

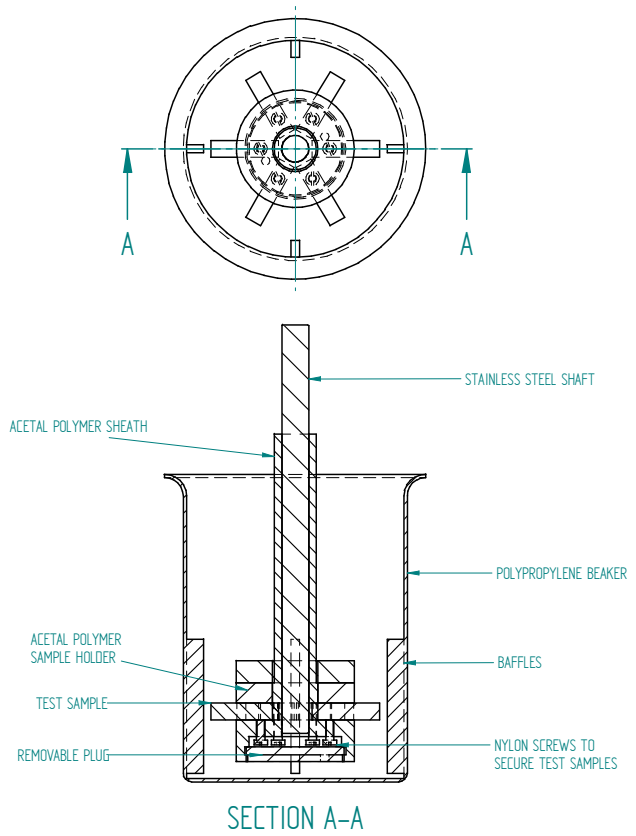

Figure 6: Sketch of the slurry pot test apparatus.

Test Slurry

The test slurry consists of a known liquid and abrasive phase, with the liquid phase being a highly alkaline liquor. The liquor was made by dissolving a known quantity of high purity aluminium wire (>99.7% pure) in a concentrated caustic solution. The wire was cleaned, rinsed and dried prior to weighing. The caustic solution was prepared using AR grade sodium hydroxide pellets (Ajax chemicals, assay 97.0%) dissolved in water which had been purified using reverse osmosis, filtering and deionisation. The aluminium was added slowly to the caustic solution and continuously stirred in a specially designed reaction vessel held at 90°C. Once all the aluminium had dissolved, the solution was cooled, filtered once through Whatman 540 grade filter paper and twice through Whatman GF/C glass microfibre filters. The resulting solution was visually clear and chemically analysed, showing the alumina concentration to be 112g/L (expressed as Na_2CO_3) and the caustic concentration to be 261g/L (expressed as Na_2CO_3).

The erodent consisted of various sized quartz particles with the proportion of each sieve range given in Table 1. The particle size ranges and concentrations were based on average data from industrial operations using slurries as the transfer mechanism between stages. The quartz particles were sourced from a local sand supplier and consisted of a mixture of angular and rounded particles. The test slurry contained 480g of abrasive particles in 720 mL of liquor, which is equivalent to approximately 40 wt% of solid to liquid.

Table 1: Particle size range of quartz particles for slurry pot testing.

Sieve Range (µm)	Wt%
0-53	72.8
53-106	5.0
106-150	5.9
150-250	5.7
250-425	5.0
425-850	4.1
850-1000	2.4
1000-1400	4.8

Slurry Pot Test Procedure

The test samples were surface ground to the desired size. For the hypereutectic weld overlay sample, Fig. 4, it was necessary to fill the check cracks with an epoxy resin to ensure that the cracks did not fill with quartz particles during testing as this would lead to errors and inconsistencies in results. This was done using standard vacuum impregnation techniques. Prior to being tested the samples wear face was wet ground to a 1200 grit finish using silicon carbide paper. This wet grinding was done in such a manner so that the scratch marks were parallel with the long axis of the sample. The samples were then degreased in acetone and hot air dried prior to weighing to an accuracy of 0.1 mg. The test samples were tested in pairs and two mild steel reference samples were included in all tests to confirm the reproducibility of the tests. The test samples were located in the rotor so that the

protrusion of the test samples was maintained at 19.0±0.1mm. The test sample holder containing the test samples was placed in the preheated slurry and coupled to the motor. The temperature of the slurry was maintained by immersion of the slurry pot in a constant temperature water bath set to 90±1°C. The duration of the slurry pot test was 5 hours. At the completion of the test, the spindle was removed and cooled in purified water. The test samples were removed and any residual slurry constituents removed by gentle rubbing with a red rubber stopper. The worn test samples were degreased in acetone and hot air dried prior to weighing. The weight loss of the sample was calculated and the test repeated to ensure consistency. The weight loss was calculated as the average of the two tests and reported relative to the weight loss of mild steel sample.

Results

The weight loss of the four alloys tested relative to mild steel is plotted in Fig. 7. The average weight loss of mild steel was 14.43 mg. The error bars indicate a conservative error of 0.5 mg relative to the weight loss of mild steel.

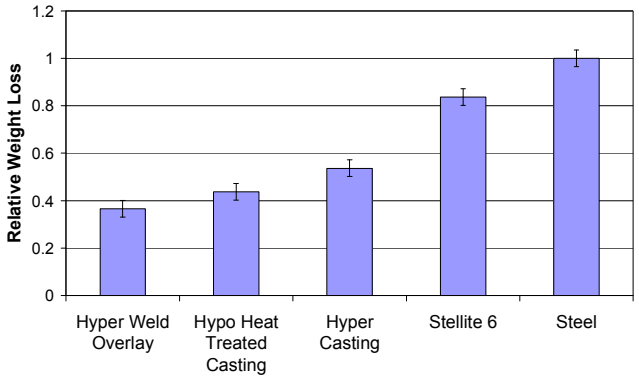

Figure 7: Slurry pot test results for the four samples tested relative to the weight loss of mild steel.

Examination of the wear surfaces was done using a field emission scanning electron microscope (FESEM). Examination of the Stellite wear surface, Fig. 8, shows a number of particle impact craters where matrix material had been extruded up and out of the impact crater. In many instances the quartz particles remain embedded in the matrix. Fig. 9 is a higher magnification of the area highlighted in Fig. 8. A particle (arrowed) can be seen at the end of the wear track. The particle was confirmed as a silica quartz particle from the slurry using energy dispersive analysis of x-rays (EDAX). The embedded quartz particle had severely plastically deformed the matrix but had not removed the matrix material by a micromachining mechanism. This is probably due to the particle not having the correct orientation, trajectory and energy for micromachining to take place.

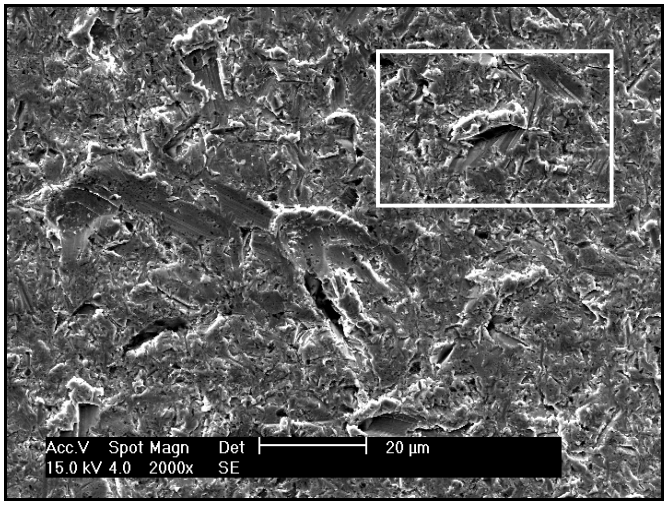

Figure 8: SEM image of the general wear surface of the Stellite 6 PTA weld overlay. A sample of the wear pattern is highlighted and shown at higher magnification in Fig. 9.

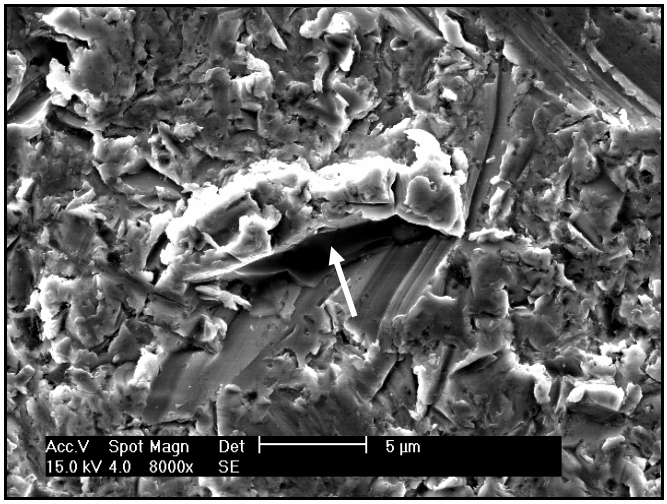

Figure 9: Higher magnification SEM image of the Stellite 6 PTA wear surface outlined by the box in Fig. 8. The above image shows the associated deformation of the matrix material by the impact and embedding of a quartz particle (arrowed).

The wear surface of the hypereutectic casting is shown in Fig. 10. It can be seen that the matrix (lighter), which is predominantly austenite, has been preferentially removed leaving the carbides exposed. It is also evident that the primary M_7C_3 carbides have undergone a form of wear with a rounding at the edges of the carbides clearly visible.

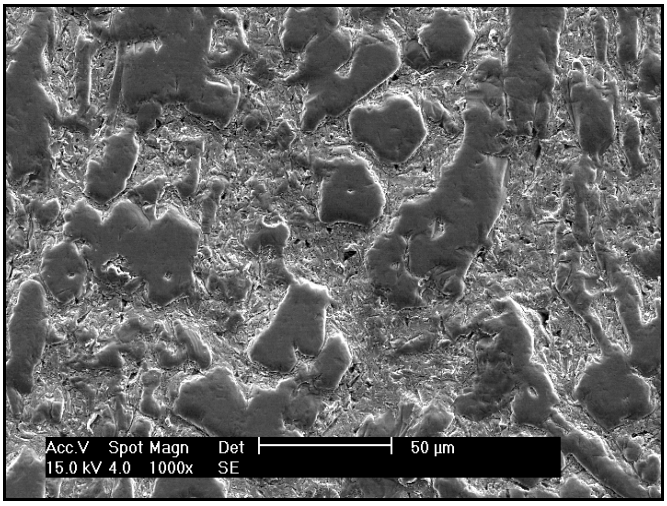

Figure 10: SEM image of the general wear surface of the hypereutectic casting.

Fig. 11 is a higher magnification image of the hypereutectic casting wear surface. The image shows a single particle impingement, which has deformed and extruded the matrix against a primary carbide. The image also further illustrates the wear associated with the primary M_7C_3 carbides with the characteristic rounding at the periphery of the exposed carbide.

Figure 11: Higher magnification SEM image of the hypereutectic casting wear surface showing a particle impingement track (arrowed) which has caused matrix deformation against a primary M_7C_3 carbide.

The wear surface of the hypoeutectic heat treated high chromium white iron casting, Fig. 12, had a distinctly different wear surface to the Stellite 6 and hypereutectic casting sample. The martensitic matrix of the hypoeutectic casting did not exhibit the degree of deformation caused by particle impingement as was the case for the Stellite 6 deposit and the hypereutectic casting. It was also apparent that the matrix of the hypoeutectic casting was not as recessed with respect to the eutectic M_7C_3 carbides as it was for the hypereutectic casting in Fig. 10. It is also apparent that the eutectic M_7C_3 carbides were rounded in a similar manner to the hypereutectic casting.

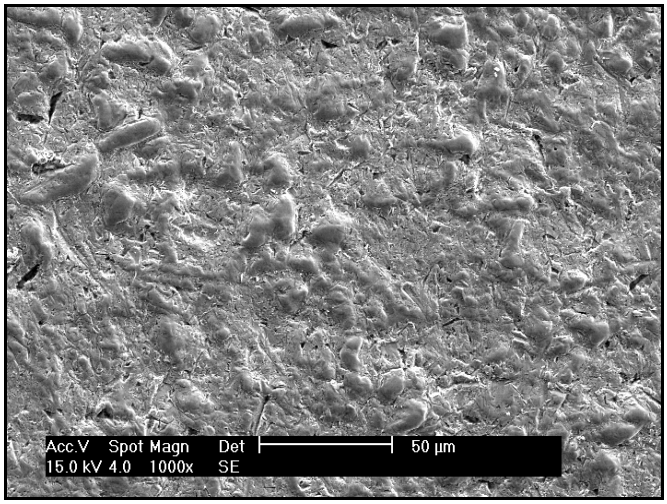

Figure 12: SEM image of the general wear surface of the hypoeutectic heat treated casting.

Fig. 13 is a higher magnification image of the hypoeutectic casting wear surface. The image shows an embedded particle, confirmed by EDAX to be quartz, and the plastic deformation of the martensitic matrix associated with the embedding of the particle.

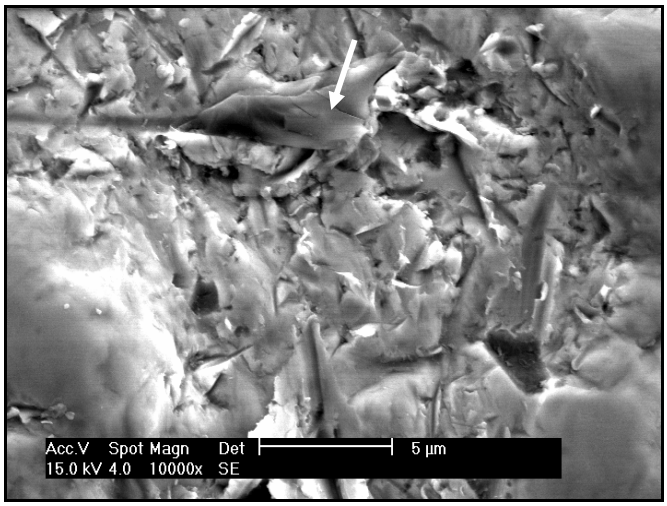

Figure 13: Higher magnification SEM image of the hypoeutectic heat treated casting wear surface showing an embedded quartz particle (arrowed) and the associated deformation of the martensitic matrix.

The distinguishing feature of the hypereutectic weld overlay wear surface, Fig. 14, is the damage that has occurred to the primary M_7C_3 carbides. In a similar manner to that observed in the hypereutectic casting, the carbides have undergone significant damage and have a rounded appearance at the

edges. The carbides are also in relief due to the removal of the austenitic matrix. Due to the close spacing of the primary carbides in the weld overlay, ploughing grooves created by impinging particles were not distinguishable in the matrix. However, Fig. 15 shows a quartz particle embedded within the matrix against a primary M_7C_3 carbide in the hypereutectic weld overlay sample.

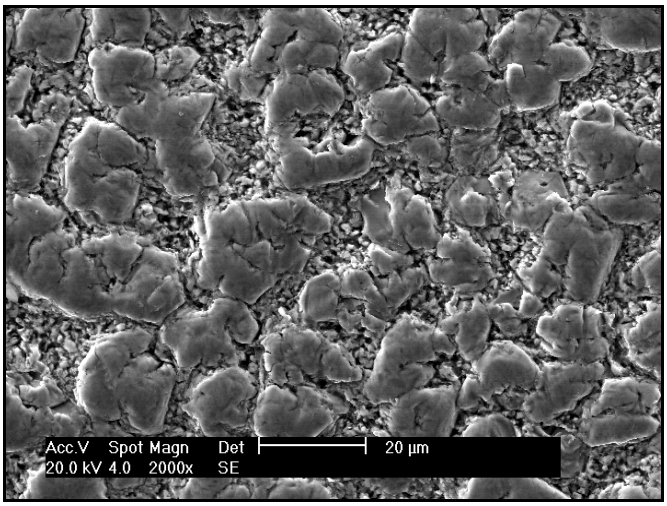

Figure 14: SEM image of the general wear surface of the hypereutectic weld overlay.

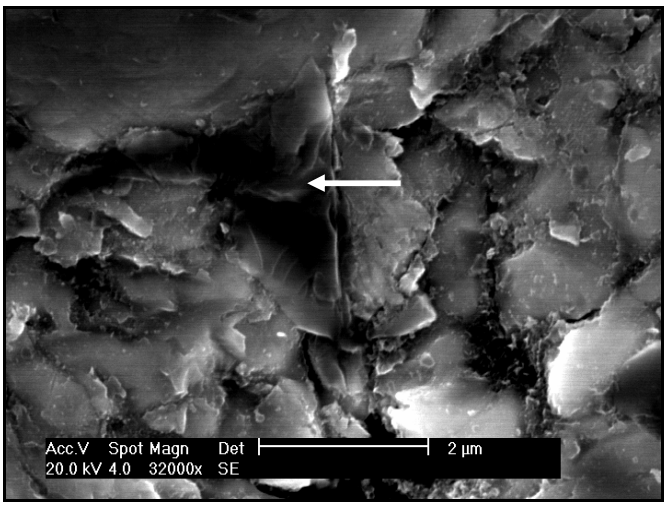

Figure 15: Higher magnification SEM image of the hypereutectic weld overlay wear surface showing and embedded quartz particle (arrowed) between primary M_7C_3 carbides.

The hardness of each of the alloys was investigated. Bulk hardness was measured using a Vickers hardness testing machine with a 30 kg load. The microhardness measurements of the M_7C_3 carbides was done using a 10g or 50g load, depending on the size of the carbides. Microhardness testing of the matrix was done using 10g, 50g, 300g. The averaged results presented in Table 2 are calculated on a minimum of 6 hardness measurements.

Table 2: Vickers hardness test results for the bulk sample and microconstituents.

Sample	Bulk	Std Dev	M_7C_3	Std Dev	Matrix	Std Dev
Stellite 6	347	9	-		384	18
Hyper Casting	682	20	1765	104	487	53
Hypo Casting	720	16	1472	285	663	26
Hyper Overlay	850	30	1484	116	-	

Discussion

The erosive wear resistance of the four alloys tested can be directly related to the bulk hardness of the alloys. The bulk hardness of unheat-treated white irons has been reported to be dependent upon carbide volume fraction [4]. However, this is not the case for white irons which have undergone a destabilisation heat treatment. The destabilisation heat treatment is commonly used to transform the austenite, primary and eutectic, to martensite and secondary carbides. This increses the bulk hardness and hence the erosive wear resistance.

The erosive weight loss of high chromium white irons is a combination of the weight loss due to matrix removal and carbide removal. In this investigation it was found that the M_7C_3 carbides, both eutectic and primary, were susceptible to wear due to the carbides having a rounded appearance. Observation of the worn surfaces found the primary and eutectic M_7C_3 carbides, of the high chromium white iron alloys, to stand proud of the bulk of the wear surface. This would indicate that they had superior wear resistance to the matrix. However, the eutectic carbides of the Stellite weld overlay could not be distinguished on the wear surface, due to their fine nature, and their contribution to wear resistance could not be determined.

The hardness of the M_7C_3 carbides is greater than that of the quartz particles (estimated to be between 900 and 1280 Vickers) [1]. The difference in hardness between the carbides and the eroding quartz particles eliminates the possibility that the carbides can be damaged due to scratching or scouring by the quartz particles. Therefore, the damage to the carbides has to occur by a chipping mechanism where small sections at the periphery of the carbide are removed by microfracture due to particle impingement. This wear mechanism is consistent with other work reported in the literature [4].

The wear of the matrix is believed to be the rate controlling factor in the erosive wear of the materials investigated. The matrix, whether soft austenite or hard martensite, showed evidence of deformation due to particle impingement. This was most pronounced in the Stellite and hypereutectic casting

samples which have a matrix hardness nearly half that of the quartz particles. The matrices of these two materials had regions of material that had been deformed by successive particle impacts or forced against a carbide by a forging mechanism to form thin highly stress regions of matrix material. These highly stressed regions of matrix material were then susceptible to fracture from further particle impact. This mechanism of erosion is consistent with the platelet mechanism of erosion reported elsewhere [7].

From the examination of the wear surfaces, the contribution of corrosion, if any, to the total wear loss could not be determined. A test apparatus that can monitor the in-situ corrosion response of the alloys under erosion-corrosion conditions would be a better way of investigating the role of corrosion. Temperature may play a crucial role in the erosion-corrosion behaviour of the tested alloys. It is known that temperature is one of the important factors controlling the rate of corrosion in many instances but the effect on erosion, if at all, is not yet known [8].

The influence of an erodent of varying sized particles and quantities on the wear rate of the alloys can not be determined conclusively from the initial slurry pot results. It is hypothesised that the presence of the larger abrasive particles would cause greater deformation of the matrix, hence, a higher wear rate. However, this raises the issue of carbide spacing and size. When the hypereutectic casting, Fig. 10, is compared with the hypereutectic weld overlay, Fig. 14, it can be seen that the spacing between the primary M_7C_3 carbides of the weld overlay is much less than the spacing between the primary M_7C_3 carbides of the hypereutectic casting. If the large abrasive particles, hypothesised to be responsible for higher matrix wear, were not capable of directly impinging on the matrix due to small carbide spacings, the wear resistance may increase. However, each of the alloys studied had primary or eutectic carbides of varying sizes. The primary carbides of the hypereutectic casting were larger than the primary carbides of the hypereutectic weld overlay. The eutectic carbides of the hypoeutectic casting were larger than the eutectic carbides of the Stellite weld overlay. It is known that the carbides wore, as the carbides developed a rounded appearance as a result of testing, but the extent to which carbide size affects the wear mechanism and wear rate of the carbides can not be determined from these test results. The investigation of carbide spacing and size will form part of an ongoing investigation of the wear mechanism of high chromium white iron alloys.

Conclusion

The developed slurry pot test device is suitable for the ranking of materials in the slurry pot erosive environment. It was found that the bulk hardness of the four alloys tested was indicative of the erosive wear resistance with the material having the highest bulk hardness wearing the least. The removal of the matrix occurs by the extrusion and forging of the matrix by particle impingement to form highly stressed regions of material that were broken off by subsequent particle impacts. The matrix removal mechanism occurs regardless of whether the matrix is soft austenite or harder martensite, however, lower wear rates are associated with martensitic matrices.

Acknowledgements

The work was undertaken as part of a Research Project for the Cooperative Research Centre for Welded Structures. Contributions were made to the project by a group of commercial sponsors.

The authors would like to thank Dr. Bernie Bednarz and Michael Fanning of CSIRO Manufacturing Science and Technology for the deposition of the Stellite PTA deposit. Additionally the authors would like to thank Rob Byrne for providing the data for the equilibrium liquor concentrations and chemical analysis of the liquors.

References

[1] Tabrett, C.P., I.R. Sare, and M.R. Ghomashchi, "Microstructure-property relationships in high chromium white iron alloys," *International Materials Reviews,* Vol. 41, No. 2 (1996), pp. 59-82.

[2] AS/NZS 2576:1996, "Welding consumables for build-up and wear resistance", *Australian/New Zealand Standard*.

[3] Thorpe, W.R. and B. Chicco, "The Fe-Rich Corner of the Metastable C-Cr-Fe Liquidus Surface," *Metallurgical Transactions A,* Vol. 16A, No. September (1985), pp. 1541-1549.

[4] Sapate, S.G. and A.V. Rama Rao, "Effect of carbide volume fraction on erosive wear behaviour of hardfacing cast irons," *Wear,* Vol. 256, No. 7-8 (2004), pp. 774-786.

[5] Pintaude, G., et al., "The particle size effect on abrasive wear of high-chromium white cast iron mill balls," *Wear,* Vol. 250-251, No. 1 (2001), pp. 66-70.

[6] Lathabai, S. and D.C. Pender, "Microstructural influence in slurry erosion of ceramics," *Wear,* Vol. 189, No. 1-2 (1995), pp. 122-135.

[7] Levy, A.V., Solid Particle Erosion and Erosion-Corrosion of Materials. ASM International (Ohio, 1995), pp. 11-25.

[8] Fontana, M.G., Corrosion Engineering, 3rd ed. McGraw Hill (1986).